

NUMERICAL SIMULATION OF CONTINUOUS BUBBLES MOTION BEHAVIOR WITH DIFFERENT LANCE SPACINGS

by

Xinting TONG, Xiaohui ZHANG*, Rui FENG, Jinhua LIN, and Hua WANG

Faculty of Metallurgical and Energy Engineering,
Kunming University of Science and Technology, Kunming, China

Original scientific paper
<https://doi.org/10.2298/TSCI220813204T>

The lance is a critical component of the bottom-blowing pool melting process, and its placement has an important impact on the pool's gas-liquid two-phase flow. In this study, a mathematical model of the bottom-blowing process is established, and the flow pattern, trajectory, wake vortex, and velocity of bubbles under four lance spacings are simulated. Results show that there are three basic bubble flow patterns appear in the flow field: bubbles coalesce before leaving the nozzle (Pattern I), bubbles coalesce after leaving the nozzle (Pattern II), and no coalescence during the rise of bubbles (Pattern III). The bubble pattern varies from Pattern I to Pattern III with the increase in lance spacing. The intensity of the influence of the wake vortex on the bubbles decreases. The Q (the Q is the second Galilean invariant of the velocity gradient tensor ∇v) value of the wake vortex is small, but the vortex structural distribution is complex. Moreover, there is a large velocity difference between gas and liquid at the beginning of gas injection, but the velocity difference between them decreases after gas injection, so the average turbulent kinetic energy in the pool initially increases sharply, and then approaches dynamic equilibrium. The top and bottom velocities of the bubbles are consistent, and the velocity fluctuation is orderly. Moreover, the greater the lance spacing is, the greater the disturbance in the pool is. The mixing effect of $D = 0.2$ m is the best among the four spacings.

Key words: double lances, lance spacing, flow pattern, wake vortex, turbulent kinetic energy

Introduction

A bottom-blowing melting furnace is a kind of copper smelting technology developed independently in China, and its melting process involves a complex multi-phase flow and heat and mass transfer [1, 2]. The gas is injected into the pool by the lance and through the melt as bubbles, thereby producing a complex gas-liquid two-phase flow. The bubbles drive the melt flow to promote heat and mass transfer between the melts [3]. Research on the multi-phase flow in the melt pool provides an improved understanding of the flow field information and a theoretical foundation for equipment and process development. Hence, the properties of bubble flow and the effect of bubbles on the liquid-phase flow field have become key research topics.

Many scholars have conducted extensive research on bubble motion, which mainly includes bubble trajectory, velocity, and deformation. Celata *et al.* [4] determined the velocity and shape of bubbles and the correlation between them. Xu *et al.* [5] obtained the bubble rise

* Corresponding author, e-mail: xiaohui.zhang@kust.edu.cn

velocity and rising trajectory through numerical simulation. Liu *et al.* [6] studied the terminal rise velocity of bubbles and determined the effects of aspect ratio and diameter on the terminal velocity of bubbles. Liu *et al.* [7] and Yan *et al.* [8] deduced from the motion characteristics of bubbles on a 2-D plane that the exact motion trajectories of bubbles in 3-D space are mainly linear, zigzag, and spiral. Cano-Lozano *et al.* [9, 10] studied the rising trajectory and wake flow of bubbles through numerical simulation, and their results showed that the unstable rise of bubbles is caused by the asymmetric shedding of the bubble wake. Cao and Macian-Juan [11] clarified the mechanism of bubble path instability by analyzing vortex dynamics and shape deformation.

Lance arrangement is one of the factors that affect the movement of bubbles. Yan *et al.* [3] reported that the reasonable inclination angle is 17° - 22° for a single-row lance and 12° - 22° for a double-row lance. Wang *et al.* [12] obtained the maximum void fraction when the double nozzle angle is 44° . Zhang *et al.* [13, 14] performed numerical simulations and orthogonal tests to optimize the structural parameters of the lance for a bath melting furnace and obtained the optimal combination of lance diameter, spacing, and inclination angle. They discovered that the effects of lance spacing, inclination, and lance size on the flow process decrease in turn. Yan *et al.* [15] investigated lance spacing in addition lance diameter and inclination angle and reported that the optimal working condition for a reduction furnace entails a spacing of 950 mm. Yu *et al.* [16] studied the effects of different nozzle structures on the flow process and found that nozzles with dispersion nozzles are beneficial to improving mixing and reaction efficiency. Yan *et al.* [17] evaluated different nozzle structures with different opening ratios. Considering the dependence on the opening ratio, they established different prediction models for the ratio of the maximum caliper distance to the hydraulic diameter of the nozzle outlet and the dimensionless bubble diameter. Li *et al.* [18] studied bubble generation characteristics by using a multi-channel lance and the homogeneity of mixing by using a multi-orifice bottom-blow lance.

In conclusion, current research on lance arrangement mostly focuses on lance number, diameter, inclination angle, and nozzle structure. Zhang *et al.* [13, 14] reported that the impact of lance spacing on the melting furnace flow process is the most essential factor. Therefore, by establishing a reasonable basic model for the bottom-blowing smelting furnace, this study applies the multi-fluid volume of fluid (VoF) model to simulate the gas-liquid two-phase flow process in the bottom-blowing smelting furnace and analyzes the flow field information by using the vortex identification method. The simulation focuses on the motion characteristics of bubbles generated by double lances with different spacings. The study also examines bubble flow pattern, motion trajectory, turbulent kinetic energy change, and velocity fluctuation. The Q-criterion identification method is used to analyze the flow field information, the vortex distribution, and its variation during bubble motion.

Model building

Numerical model

The multi-fluid VoF model

In this paper, the Eulerian multi-fluid VoF model is used, which combines the respective advantages of Eulerian and VoF methods, and it can simulate many more complex flows and has been widely used in the field of multi-phase flow. The multi-fluid VoF model allows modelling of both dispersed and sharp interfaces while still being able to provide different velocity fields for each phase. The volume fraction equation, like the VoF model, can be solved with implicit or explicit temporal discretization. Assuming no mass transfer between the two-phases, the conservation equation in this approach is [19-23]:

The continuity equation is given:

$$\frac{\partial}{\partial t}(\alpha_i \rho_i) + \nabla(\alpha_i \rho_i \vec{v}_i) = 0 \quad (1)$$

where α_i , ρ_i , and v_i are the volume fraction, density and velocity vector of phase i , respectively.

The form of the momentum equation:

$$\frac{\partial}{\partial t}(\alpha_i \rho_i \vec{v}_i) + \nabla(\alpha_i \rho_i \vec{v}_i \vec{v}_i) = -\alpha_i \nabla p + \nabla \bar{\tau}_i + \alpha_i \rho_i \vec{g} + \sum \vec{F} + \vec{R}_{ki} \quad (2)$$

$$\sum \vec{F} = \vec{F}_i + \vec{F}_{\text{lift},i} + \vec{F}_{\text{wl},i} + \vec{F}_{\text{vm},i} + \vec{F}_{t,i} \quad (3)$$

where p is the pressure, $\bar{\tau}_i$ – the stress-strain tension of the i phase, \vec{g} – the acceleration of gravity, $\sum F$ – the force on phase i , including external body force, lift force, wall sliding force, virtual mass force, and turbulent dispersion force, and \vec{R}_{ki} – the interaction force between the two-phases. It is important to note that $\sum \alpha_i = 1$. Similar equations can be constructed for phase k . The interaction force between the two-phases, \vec{R}_{ki} , is defined:

$$\vec{R}_{ki} = K_{ki} (\vec{v}_k - \vec{v}_i) \quad (4)$$

The aforementioned equation represents the average interphase momentum exchange, excluding any effect caused by turbulence, and K_{ki} represents the interfacial momentum exchange coefficient, defined:

$$K_{ki} = \frac{\alpha_k \alpha_i \rho_k}{\tau_k} f \quad (5)$$

where f is the drag function and τ_k is the *particle relaxation time*. In the multi-fluid VoF model, the symmetric and anisotropic drag laws are specified, and the drag can be large enough to balance the velocities of the two-phases at the interface. The symmetric drag law is isotropic, and for higher drag coefficients, it tends to approach the behavior of the single VoF model. The anisotropic drag law profits to overcome the drawback of symmetric drag by allowing sharp-angle interfaces to have higher drag coefficients in the normal direction and lower drag coefficients in the tangential direction.

The Q criteria method

In this paper, the Q criterion is used to identify and analyze the flow field of the bottom blowing model, relying on the velocity gradient tensor decomposition, where the velocity gradient tensor ΔV :

$$\nabla V = \frac{1}{2}(\nabla V + \nabla V^T) + \frac{1}{2}(\nabla V - \nabla V^T) = \mathbf{A} + \mathbf{B} \quad (6)$$

where \mathbf{A} and \mathbf{B} in the previous equation represent the symmetric part (symmetric tensor) and the antisymmetric part (antisymmetric tensor) of the velocity gradient tensor, respectively, and then the Q is defined [24-26]:

$$Q = \frac{1}{2}(\|\mathbf{B}\|_F^2 - \|\mathbf{A}\|_F^2) \quad (7)$$

where $\|\cdot\|_F$ is the Frobenius norm of the matrix. The symmetric tensor \mathbf{A} has the effect of resisting the rotation of the anti-symmetric tensor \mathbf{B} . Therefore, the physical significance of Q lies in the fact that the vortex structure not only requires the existence of vortices (anti-symmetric tensor \mathbf{B}) but furthermore requires that the anti-symmetric tensor \mathbf{B} can overcome the deformation

effect represented by the symmetric tensor A . The $Q > 0$ indicates that the existence of vortex is a good indicator of turbulent structure. From the perspective of energy, the magnitude of Q actually represents the energy of unit mass vortex and unit space vortex [27, 28].

Application model validation

Many scholars have verified that the application of the Eulerian multi fluid VoF model in the study of gas-liquid two-phase flow is feasible, and the model is widely used in the study of multi-phase flow in various scenarios [29-31]. Song and Jokilaakso [32] used the Eulerian multi fluid VoF model to simulate multi-phase flow in bottom blown copper smelting furnace, and used a water model experiment to verify the correctness of the mathematical model, as shown in fig. 1. Our study is based on the multi-lance simulation of the bottom blown smelting furnace, which is similar to the research of [32].

Xu *et al.* [33], Xu *et al.* [34], and Li *et al.* [35] in our research group have experimentally verified the calculation results of using the Eulerian VoF model to simulate the rise of bubbles generated by a single lance, as shown in fig. 1(b). As the verification part has been discussed in detail in other papers of the research group, this article will not discuss it.



Figure 1. Verification of mathematical model; (a) verification of multi-lance for bottom blowing [32] and (b) verification of single lance model for bottom blowing [34]

Physical model and grid-independent verification

Physical model

In this paper, the bottom-blown copper bath melting furnace is used as the research background to establish the physical model. The physical model used for simulation is based on the laboratory cold experimental model, which is simplified to a cylinder of 1 m in height and 1.6 m in diameter. The bottom-blown submerged lance has an inner diameter of 0.018 m and a submerged depth of 0.02 m, with air inside the tube. The physical model and computational domain boundaries are shown in fig. 2. The physical properties of the liquid in the pool refer to those of Deng *et al.* [36], as shown in tab. 1.

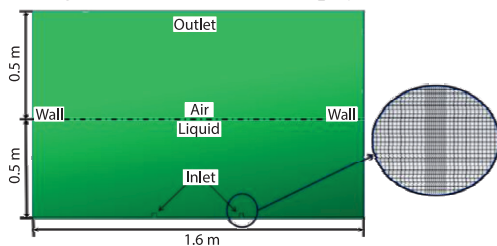


Figure 2. Physical model and computational domain boundaries

Table 1. The physical properties of the liquid in the pool

	Density [kgm^{-3}]	Viscosity [$\text{Pa}\cdot\text{s}$]	Surface tension [Nm^{-1}]
Liquid	4440	0.004	0.33

Grid-independent verification and solution set-up

The influence of different grid numbers on the bubble rise is explored by simulating the bubble creation process while the lance spacing is 0.2 m. It can be seen from fig. 3 that the time required for the bubbles to travel from the bottom of the pool to the liquid surface is essentially the same when the grid number reaches $12 \cdot 10^5$ or more. Considering the calculation load and accuracy, the grid number of $12 \cdot 10^5$ is chosen for simulation.

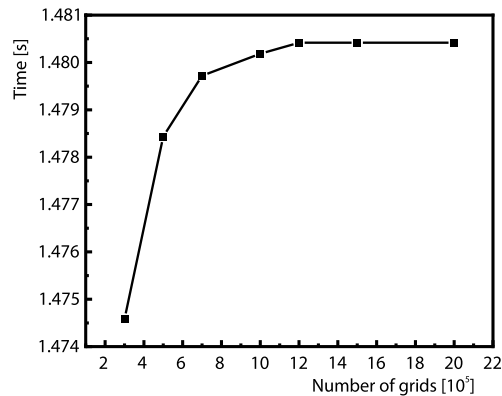


Figure 3. Grid-independent verification

The bottom-blow lance tube is filled with air, with a gas velocity of 0.5 m/s at its inlet, the outlet is set to pressure-outlet, and the solid wall is treated as a no-slip boundary. The standard wall function treatment is used for processing within the boundary-layer near the wall, and the Standard *k-ε* model is selected for the turbulence model. Table 2 shows the setting parameters of the center distance between the two lances.

Table 2. Lance spacing setting

Lance spacing, <i>D</i> [m]	0.05	0.1	0.2	0.4
-----------------------------	------	-----	-----	-----

Results and discussion

Bubble flow pattern

By simulating the bubble generation and rising process of the double lances with different spacings, different bubble flow patterns are obtained when the gas-liquid two-phase flow reaches stability. We summarize the bubble flow patterns into three main types in accordance with the bubble coalescence behavior during the rising process, fig. 4. The three main flow patterns are: (I) bubbles coalesce before leaving the nozzle, (II) coalescence occurs after disengagement from the nozzle, and (III) two bubbles separate from the nozzle without coalescence and rise separately. The three flow patterns obtained from the simulations are in general agreement with the description of bubble flow patterns mentioned by Yang *et al.* [37].

Lance spacing affects the flow patterns of bubbles. As the lance spacing increases, the bubble flow pattern exhibits a gradual change from flow Pattern I to flow Pattern III during the process of continuous bubble generation. When the lance spacing is large enough, the interaction between bubbles is small, and the flow pattern is always maintained as flow Pattern III.

In fig. 4(a), the two bubbles aggregate and form a large bubble before exiting the nozzle. The bubble flow pattern is always flow Pattern I.

In figs. 4(b) and 4(c), the generated bubbles rise away from the nozzle, presenting a process of approaching and then moving away until collapsing at the liquid surface (flow Pattern III). With the blowing process, the liquid in the pool changes from being relatively static to being chaotic due to the influence of the bubbles; such a change affects the bubbles. The bubbles generated by the two nozzles coalesce on the rising path (flow Pattern II). The degree of disturbance in the pool deepens, and the location of bubble coalescence becomes gradually low until the bubbles coalesce before detaching from the nozzle (flow Pattern I).

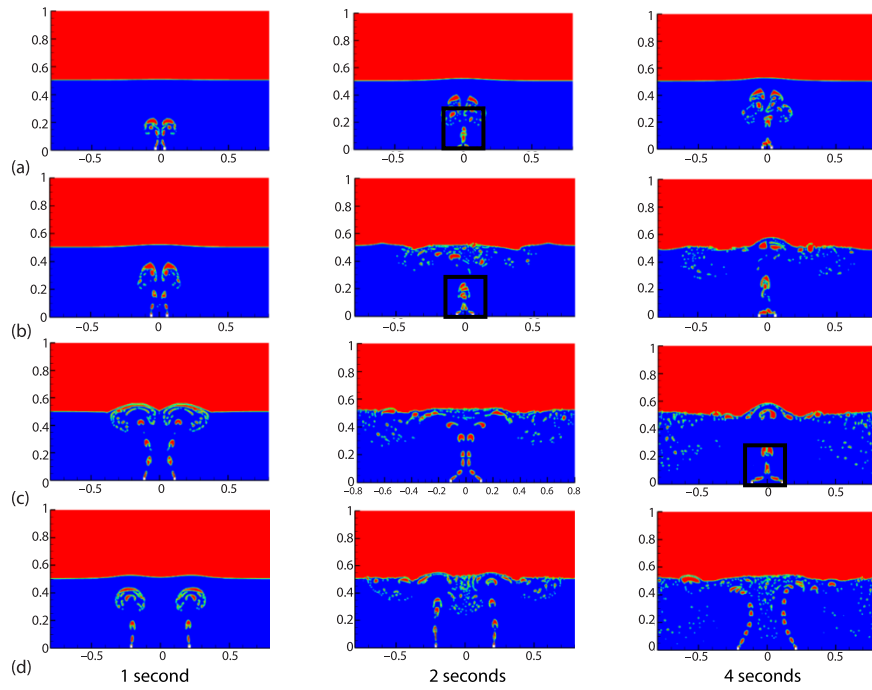


Figure 4. Continuous bubble change phase diagram; (a) $D = 0.05$ m, (b) $D = 0.1$ m, (c) $D = 0.2$ m, and (d) $D = 0.4$ m

As shown in fig. 4(d), when the spacing is $D = 0.4$ m, the continuous bubbles always maintain a certain distance from the nozzle during the rising process and collapse at the liquid level. With the continuous stirring of the bubbles to the liquid in the pool, the bubbles tend to approach then move away from each other during the rising process, but no bubble coalescence occurs (flow Pattern III).

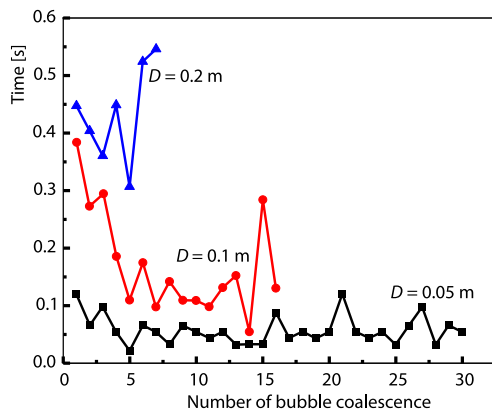


Figure 5. Coalescence time and number of coalesced bubbles in the pool

The bubble flow pattern and bubble coalescence are affected by lance spacing. As demonstrated in fig. 5, the coalescence time and quantity of coalescence bubbles vary for different lance spacings. The figure indicates that the time of bubble coalescence is proportional to the lance spacing, D , and the number of coalesced bubbles is inversely proportional to D . The larger lance spacing, D , is, the longer the time required for bubble coalescence is, the smaller the number of coalesced bubbles is, and the lower the coalescence possibility is.

Bubble trajectory and wake vortex

The bubble trajectory diagram can reflect the interaction between bubbles. In this study, the whole trajectory of bubbles is plotted by the position of the largest volume of bubble shape center after bubble coalescence or fragmentation, fig. 6. As shown in the figure, the tra-

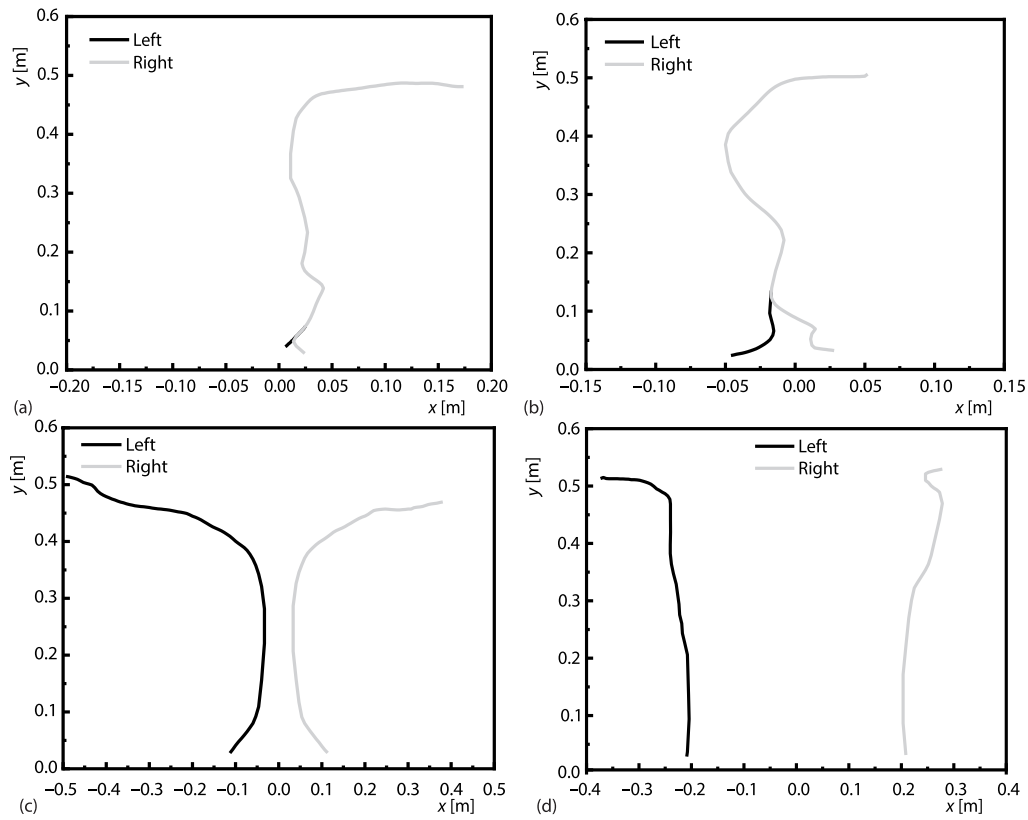


Figure 6. The trajectory of bubbles in the pool; (a) $D = 0.05$ m, (b) $D = 0.1$ m, (c) $D = 0.2$ m, and (d) $D = 0.4$ m

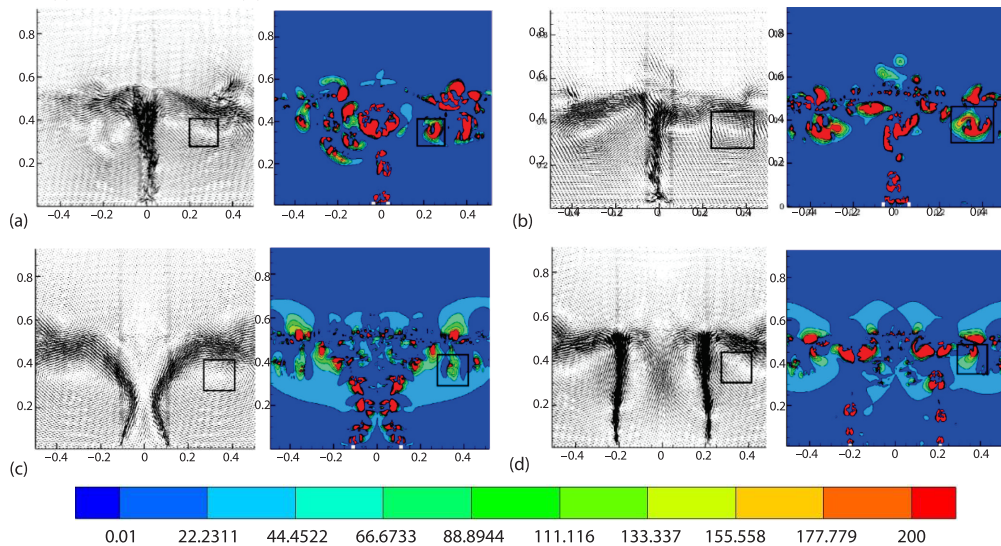


Figure 7. Velocity vector and Q -criteria diagram in the pool at 2 seconds; (a) $D = 0.05$ m, (b) $D = 0.1$ m, (c) $D = 0.2$ m, and (d) $D = 0.4$ m

jectory of bubbles is zigzag and wobbly. The closer the lances are arranged, the easier the bubble coalescence will occur, the tracks of the two bubbles shown in figs. 6(a) and 6(b) coincide, which is consistent with the results reflected in fig. 5. However, when $D = 0.1$ m, the trajectory oscillation after bubble coalescence is relatively intense.

In addition, when the lance spacing $D = 0.2$ m, fig. 6(c), the lateral displacement of the two bubbles is the largest, and the bubbles attract each other. When the spacing $D = 0.4$ m, fig. 6(d), the two bubbles do not coalesce, and the lateral displacement is not large. Therefore, the influence of interaction between bubbles decreases with the increase of D .

Figure 7 shows the velocity vector distribution and Q criterion diagram in the flow field at 2 seconds under four conditions. The air is injected into the pool with a certain initial velocity, and the bubbles push the surrounding liquid to the outside to achieve momentum transfer from the bubbles to the liquid. The fluid around the bubble flows in all directions, but the direction is deflected, as shown on the left side of fig. 7. The vortex is caused by the pressure difference in the flow field. According to the Bernoulli effects, the bubbles are attracted to each other after leaving the two nozzles. Thus, the flow pattern evolution mentioned previously, fig. 4, and unstable rising path, fig. 5, are generated. However, the influence of the wake vortex on bubbles is limited by the lance spacing. As shown in fig. 7(d), the bubbles are essentially not affected by the pressure difference when the spacing is large.

As illustrated on the right side of fig. 7, the introduction of the Q criterion vortex identification method reflects that left-right symmetric vortices exist in the flow field around the bubble. The Q contours in the figure show a gradient distribution, with the largest Q value at the center of the vortex structure. Figures 7(a) and 7(b) show that there are vortices with small structures but large Q value in the flow field, and the middle and lower parts of the flow field are not stirred. When $D = 0.2$ m and $D = 0.4$ m, figs. 7(c) and 7(d), the vortex dissipation increases due to the collision between fluids. Thus, vortex structures with small Q value and more complex distribution are present in the flow field. To sum up, the influence ability of the wake vortex on bubbles decreases as the lance spacing increases. However, the influence of the vortex on the liquid is enhanced, mainly in the increase of liquid confusion, to avoid the problem that the dead zone in the pool cannot be stirred.

Turbulent kinetic energy and bubble velocity variation

The turbulent kinetic energy of the liquid in the pool under four conditions is compared and analyzed, fig. 8. From the overall trend, the turbulent kinetic energy rises dynamical-

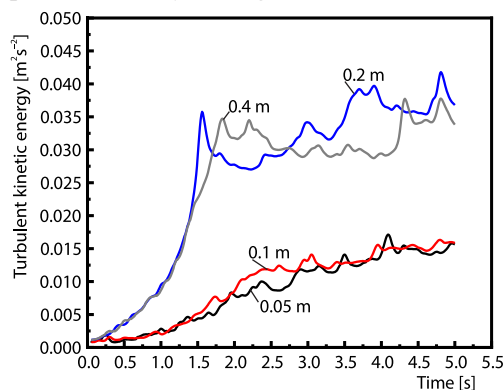


Figure 8. Variation of turbulent kinetic energy for four working conditions in the pool

ly. The turbulent kinetic energy with $D = 0.05$ m and $D = 0.1$ m showed a steady upward trend. However, when $D = 0.2$ m and $D = 0.4$ m, the change of turbulent kinetic energy is more intense than that in the other two conditions. This indicates that increasing the spacing between the lance can improve the mixing effect of liquid. According to the figure, the turbulent kinetic energy in the liquid with $D = 0.2$ m and $D = 0.4$ m rises sharply within 0-1.8 seconds, and the former first reaches the peak. After reaching the peak, the turbulent kinetic energy of both conditions decreases, but the turbulent kinetic energy of $D = 0.4$ m is higher than that of $D =$

0.2 m at 2.25-2.76 seconds. After 2.75 seconds, the turbulent kinetic energy with $D = 0.2$ m shows a substantial oscillation upward trend. Conversely, the turbulent kinetic energy with $D = 0.4$ m is in dynamic equilibrium until 4.2 seconds, after which it slowly increases. According to figs. 7 and 8, the vortex structure distribution is the most complex, the increase of turbulent kinetic energy is the most intense, and the ability of gas-liquid mixing and stirring is the best when the lance spacing $D = 0.2$ m.

A close relationship exists between turbulent kinetic energy and velocity fluctuation, namely, the higher the turbulent energy is, the higher the velocity fluctuation is. Figure 9 shows the top and bottom velocity variations of the continuous bubbles, and the overall velocity fluctuation is reflected by the velocity fluctuation at the top and bottom of the bubbles. The bottom velocity of the two bubbles changes more violently than the top velocity when the lance spacing is $D = 0.05$ m and $D = 0.1$ m, figs. 9(a) and 9(b). Under the two conditions, because of the instability caused by the coalescence of the left and right bubbles, the bubble velocity change is fluctuant and disordered.

As shown in fig. 9(c), the trends of the top and bottom velocities of the generated bubbles are the same when $D = 0.2$ m, with the velocities reaching the maximum near 3.4 seconds then decreasing to the minimum near 3.55 seconds and slowly increasing afterward.

As shown in fig. 9(d), the overall velocity trend of the bubbles generated by lance spacing $D = 0.4$ m is consistent, with a small increase in each velocity, followed by a steady decrease at about 3.1 seconds and basic stability after 3.4 seconds.

Figures 7-9 indicate that turbulent kinetic energy is the most violent, velocity oscillation is the most orderly, and the vortex distribution in the flow field is the most complex when lance spacing D is 0.2 m, as a result, the liquid in the pool is stirred the most extensively.

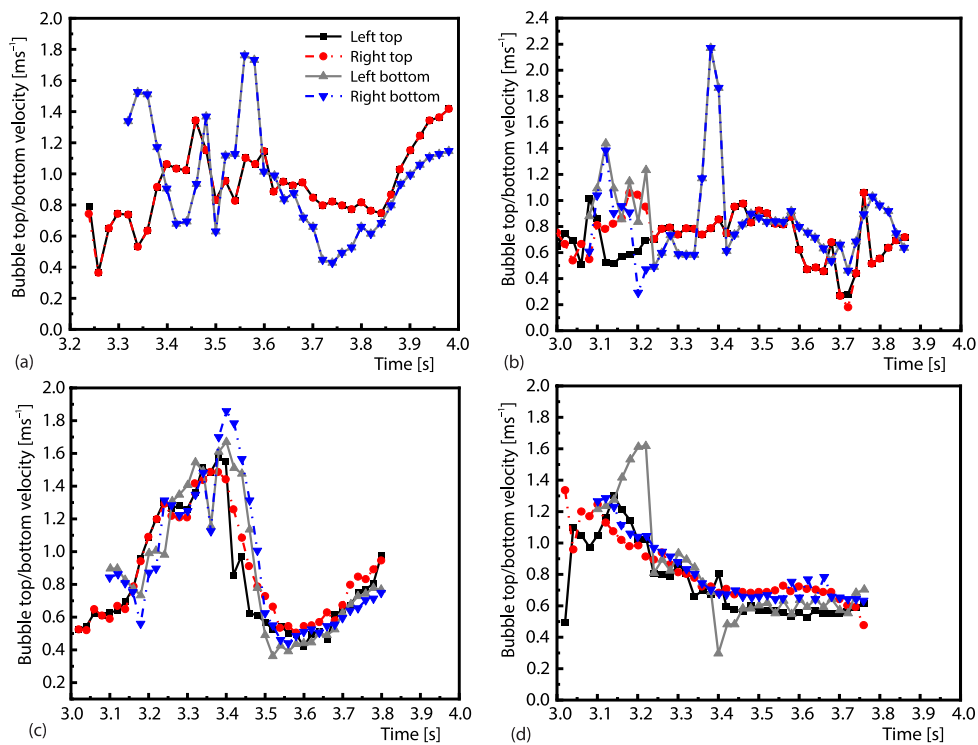


Figure 9. Variation of bubble velocity in the pool; (a) $D = 0.05$ m, (b) $D = 0.1$ m, (c) $D = 0.2$ m, and (d) $D = 0.4$ m

Conclusions

In this study, the multi-fluid VoF model is used to simulate the motion of continuous bubbles under four different lance spacings. The flow patterns, rising trajectories, turbulent kinetic energy, and velocity fluctuations during the rise of continuous bubbles are obtained. The conclusions are as follows.

- The continuous bubble flow patterns produced by the double lances can be divided into three types according to whether the bubbles coalesce and where they coalesce. With the increase in lance spacing, the flow pattern shows a trend from flow Pattern I to flow Pattern III.
- The wake vortex is generated during the ascent of the bubbles. The stronger the wake vortex is, the stronger the attraction between bubbles is. With the increase in lance spacing, as shown in the Q -criterion diagram, the distribution of the wake vortex becomes increasingly complex, the degree of disturbance in the liquid is increased, and the dead zone in the pool is reduced.
- With the increase in lance spacing, the turbulence intensity in the pool is significantly increased, and the top and bottom velocity changes of the continuous bubbles gradually become consistent. When the spacing, $D = 0.2$ m, the increase in turbulent kinetic energy is the most intense, and the change in bubble top and bottom velocities is the most regular and intense.
- Comprehensive analysis of the Q -criterion diagram, turbulent kinetic energy change, and bubble velocity change shows that the dead zone in the pool is minimized and the mixing effect is the best when $D = 0.2$ m.

Acknowledgment

This work was supported by the Yunnan Fundamental Research Projects (No. 202101AT070120, No. 202301AT070469), the Yunnan Major Scientific and Technological Projects (No. 202202AG050002-2), and the National Natural Science Foundation of China under Contract (No. 51966005). We also thank Siyao Li for her help in this research.

References

- [1] Qu, S., et al., Discussion on Production Practice of Oxygen-Enriched Bottom-Blown Smelting and Design Improvement of Bottom-Blown Furnace (in Chinese), *Zhongguo Youse Yejin*, 41 (2012), 1, pp. 10-13
- [2] Chen, S. P., et al., Summarize on the Technology of Copper Pyrometallurgy (in Chinese), *Tongye Gongcheng*, 4 (2010), pp. 44-49
- [3] Yan, H. J., et al., Influence of Lance Arrangement on Bottom-Blowing Bath Smelting Process (in Chinese), *The Chinese Journal of Non-ferrous Metals*, 22 (2012), 8, pp. 2393-2400
- [4] Celata, G. P., et al., Measurements of Rising Velocity of a Small Bubble in a Stagnant Fluid in one- and two-Component Systems, *Experimental Thermal and Fluid Science*, 31 (2007), 6, pp. 609-623
- [5] Xu, L. J., et al., Numerical Simulation of the Dynamics of Single Bubble Behavior in Still Water (in Chinese), *Journal of Yangtze River Scientific Research Institute*, 28 (2011), 9
- [6] Liu, L., et al., Experimental Studies on the Terminal Velocity of Air Bubbles in Water and Glycerol Aqueous Solution, *Experimental Thermal and Fluid Science*, 78 (2016), Nov., pp. 254-265
- [7] Liu, L., et al., Experimental Studies on the Shape and Motion of Air Bubbles in Viscous Liquids, *Experimental Thermal and Fluid Science*, 62 (2015), Apr., pp. 109-121
- [8] Yan, H. J., et al., Experimental Study on Shape and Rising Behavior of Single Bubble in Stagnant Water (in Chinese), *Journal of Central South University (Science and Technology)*, 47 (2016), 7, pp. 2513-2520
- [9] Cano-Lozano, J. C., et al., Wake Instability of a Fixed Axisymmetric Bubble of Realistic Shape, *International Journal of Multi-phase Flow*, 51 (2013), May, pp. 11-21
- [10] Cano-Lozano, J. C., et al., Paths and Wakes of Deformable Nearly Spheroidal Rising Bubbles Close to the Transition Path Instability, *Physical Review Fluids*, 1 (2016), 5,
- [11] Cao, Y., Macian-Juan, R., Numerical Investigation of Hot and Cold Bubbles Rising in Water, *Nuclear Engineering Design*, 382 (2021), 3, 111390
- [12] Wang, D. X., et al., Water Model Study of Bubble Behavior in Matte Smelting Process with Oxygen Bottom Blowing (in Chinese), *Journal of Northeastern University*, 34 (2013), 12, pp. 1755-1758

- [13] Zhang, Z. Y., et al., Numerical Simulation of Gas-Liquid Multi-Phase Flows in Oxygen Enriched Bottom-Blown Furnace (in Chinese), *Chinese Journal of Non-ferrous Metals*, 22 (2012), 6, pp. 1826-1834
- [14] Zhang, Z. Y., et al., Optimization Analysis of Lance Structure Parameters in Oxygen Enriched Bottom-Blown Furnace (in Chinese), *Zhongguo Youse Jinshu Xuebao/Chinese Journal of Non-ferrous Metals*, 23 (2013), 5, pp. 1471-1478
- [15] Yan, H. J., et al., Numerical Simulation and Structural Optimization of Gas-Liquid two-Phase Flow in Reduction Furnace of Lead-Rich Slag (in Chinese), *The Chinese Journal of Non-ferrous Metals*, 24 (2014), 10, pp. 2642-2651
- [16] Yu, Y., et al., Hydraulic Model Experiment and Numerical Simulation of Bottom-Blowing Copper Smelting Furnace, *Applied Mechanics and Materials*, 602-605 (2014), Aug., pp. 546-553
- [17] Yan, H.-J., et al., Cold Model on Bubble Growth and Detachment in Bottom Blowing Process, *Transactions of Non-Ferrous Metals Society of China*, 29 (2019), 1, pp. 213-221
- [18] Li, S., et al., Strengthening Mechanism Analysis and Evaluation Methods of Multi-Channel Bottom-Blowing Spray Lance Stirring, *Fuel Cells*, 21 (2021), 1, pp. 99-108
- [19] Parsi, M., et al., Assessment of a Hybrid CFD Model for Simulation of Complex Vertical upward Gas-Liquid Churn Flow, *Chemical Engineering Research and Design*, 105 (2016), Jan., pp. 71-84
- [20] Guerrero, E., et al., Comparison between Eulerian and VOF Models for Two-Phase Flow Assessment in Vertical Pipes, *Ct and F-Ciencia Tecnologia Y Futuro*, 7 (2017), 1, pp. 73-83
- [21] Zahedi, P., et al., The CFD Simulation of Multi-Phase Flows and Erosion Predictions under Annular Flow and Low Liquid Loading Conditions, *Wear*, 376-377 (2017), Part B, pp. 1260-1270
- [22] Chen, G., et al., Assessment of an Eulerian Multi-Fluid VOF Model for Simulation of Multi-Phase Flow in an Industrial Ruhrstahl-Heraeus Degasser, *Metallurgical Research and Technology*, 116 (2019), 6, pp. 1-10
- [23] Akhlaghi, M., et al., Multi-Fluid VoF Model Assessment to Simulate the Horizontal Air-Water Intermittent Flow, *Chemical Engineering Research and Design*, 152 (2019), Dec., pp. 48-59
- [24] Hunt, J. C. R., et al., Eddies, Streams, and Convergence Zones in Turbulent Flows, Studying Turbulence Using Numerical Simulation Databases, *Proceedings*, 2nd of the 1988 Summer Program, NASA, Washington D.C., USA, 1988
- [25] Liu, C., Liutex-Third Generation of Vortex Definition and Identification Methods (Article), *Kongqi Donglixue Xuebao/Acta Aerodynamica Sinica*, 38 (2020), 3, pp. 413-431
- [26] Wang, Y., Gui, N., A Review of the Third-Generation Vortex Identification Method and Its Applications, *Journal of Hydrodynamics (Ser. A)*, 34 (2019), 4, pp. 413-429
- [27] Fu, W. S., et al., Estimation of Turbulent Natural-Convection in Horizontal Parallel Plates by the Q Criterion, *International Communications in Heat and Mass Transfer*, 45 (2013), July, pp. 41-46
- [28] Zhou, H., et al., Research of Wall Roughness Effects Based on Q Criterion, *Micro-Fluidics and Nanofluidics*, 21 (2017), 7, 114(1)
- [29] Kulju, T., et al., Validation of Three-Phase CAS-OB CFD-Model, *IFAC-PapersOnLine*, 48 (2015), 17, pp. 1-5
- [30] Zhao, S. L., et al., Performance Test and Flow Pattern Simulation of Small Diameter Thermosyphons, *Advances in Chemical, Material and Metallurgical Engineering*, 634-638 (2013), 1, pp. 3782-3787
- [31] Vincent, S., et al., Penalty and Eulerian-Lagrangian VOF Methods for Impact and Solidification of Metal Droplets Plasma Spray Process, *Computers and Fluids*, 113 (2015), May, pp. 32-41
- [32] Song, K., Jokilaakso, A., The CFD Modelling of Multi-Phase Flow in an SKS Furnace: The Effect of Tuyere Arrangements, *Metallurgical and Materials Transactions B*, 52 (2021), 3, pp. 1772-1788
- [33] Xu, J. R., et al., Effect of Bed Shrinkage on Iron Ore Sintering Process, *Aip Advances*, 12 (2022), 6,
- [34] Xu, J. R., et al., Flow and Heat Transfer Characteristics of High Temperature Continuous Rising Bubbles, *Thermal Science*, 26 (2022), 4B, pp. 3317-3324
- [35] Li, S. Y., et al., Numerical Simulation of Flow and Heat Transfer Characteristics of Methane Immersion Combustion Process (in Chinese), *China Water Transport*, 21 (2021), 04, pp. 42-44
- [36] Deng, W. P., et al., Numerical Simulation of Biodiesel Submerged Combustion in Copper Bath Smelting Process (in Chinese), *The Chinese Journal of Non-ferrous Metals*, 29 (2019), 12
- [37] Yang, H., et al., Continuous Formation and Coalescence of Bubbles through Double-Nozzle in Non-Newtonian Fluid (in Chinese), *Chemical Engineering (China)*, 44 (2016), 8, pp. 37-41